Research Article

High CO Adsorption Performance of CuCl-Modified Diatomites by Using the Novel Method "Atomic Implantation"

Manh B. Nguyen [iD],[1,2] **Tuyen V. Nguyen** [iD],[1] **Giang H. Le** [iD],[1] **Trang T. T. Pham,**[1] **Khu Le Van** [iD],[3] **Giang T.T. Pham,**[4] **Tung Ngoc Nguyen** [iD],[5] **Quang Vinh Tran** [iD],[1] **and Tuan A. Vu** [iD][1]

[1]*Institute of Chemistry, Vietnam Academy of Science and Technology (VAST), 18 Hoang Quoc Viet Street, Cau Giay, Ha Noi, Vietnam*
[2]*Institute of Research and Development, Duy Tan University, Da Nang 550000, Vietnam*
[3]*Faculty of Chemistry, Hanoi National University of Education (HNUE), Hanoi 100000, Vietnam*
[4]*Faculty of Chemical Technology, Hanoi University of Industry (HUI), 298 Minh Khai Bactuliem, Ha No. 100000, Vietnam*
[5]*Center for Research and Technology Transfer, Vietnam Academy of Science and Technology (VAST), 18 Hoang Quoc Viet Street, Cau Giay, Ha Noi, Vietnam*

Correspondence should be addressed to Manh B. Nguyen; nguyenbamanh@duytan.edu.vn and Tuan A. Vu; vuanhtuan.vast@gmail.com

An atomic implantation method was used to modify diatomite with CuCl. The CuCl/diatomite samples were characterized by different techniques, including FTIR, XRD, BET, SEM-TEM, EDX, and CO-TPR. Characterization results revealed the formation of CuCl particles of 50–60 nm highly dispersed on diatomite surface. CO adsorption measurements showed that 2CuCl/diatomite exhibits the highest CO adsorption capacity among all CuCl-modified samples with diatomite. Its CO adsorption capacity of 2.96 mmol/g at 30°C is 10 times higher than that of unmodified diatomite (0.29 mmol/g). The CO adsorption on CuCl-modified diatomites was found to fit well with the Langmuir–Freundlich model.

1. Introduction

Carbon monoxide (CO) is a toxic gas and metabolic waste, which is produced from the incomplete combustion of carbonaceous substances in coal stoves, thermal power plants, automobile engines, etc. [1–4]. CO poisoning is dangerous to human health because it reacts with hemoglobin in the blood to form carboxy-hemoglobin, which limits the transportation of oxygen in the blood and consequently it may cause the death [5]. Therefore, researchers are now interested in high-efficiency carbon monoxide removal technology. Among many methods for CO removal, adsorption is widely used due to its high efficiency and low-cost treatment. Adsorbents for selective carbon monoxide adsorption such as metal-organic frameworks, zeolite, activated carbons, grapheme, and metal oxides have been

reported in the literature [6–15]. Recently, Manh et al. [13] reported that graphene oxide modified with Cu (I) showed much higher CO adsorption capacity than that of unmodified graphene oxide. The formation of π-complexation bond between Cu (I) ions molecules and CO on the adsorbent surface could improve CO adsorption selectivity. Thus, CO adsorption capacity of graphene oxide increased from 0.38 mmol/g to 2.9 mmol/g with CuCl modification. Xue et al. [14] synthesized CuCl-modified activated carbon (CuCl/AC), which showed a high CO adsorption capacity of 45.4 cm³/g, 4 times higher than that of activated carbon (11.5 cm³/g). Doping carbon xerogels with CuCl also found to significantly increase its CO adsorption capacity [15]. He et al. [12] synthesized the CuCl/MCM-41, ZnCl$_2$/MCM-41, and Zn–Cu (I)/MCM-41 materials for CO adsorption. The author reported that the materials CuCl/MCM-41, ZnCl$_2$/

MCM-41, and Zn–Cu (I)/MCM-41 have CO adsorption capacity of 0.59 mmol/g, 0.26 mmol/g, and 1.82 mmol/g, respectively. Gao et al. [8] investigated the CO adsorption on the CuCl supported AC and showed high CO (3.63 mmol/g) adsorption capacity and high CO/CO_2, CO/CH_4, and CO/N_2 adsorption selectivity. Xie et al. [16] found that modifying zeolite with CuCl increases CO selectivity from a CO and CO_2 mixture at a temperature higher than room temperature. When polystyrene resin with amine groups was modified with CuCl, its CO adsorption capacity increased 5.7 times [17].

Currently, clay minerals such as halloysite, dolomite, bentonite, Ilmenite, and diatomite have attracted a lot of interest because of their potential application or environmental treatment [18–22]. Clay-based adsorbents for adsorption of gases such as CO, CO_2, CH_4, H_2S, heavy metal ions, and organic pollutants were also investigated. Volzone et al. [23] investigated the adsorption of CO, CO_2, and SO_2 gases on HCl-treated bentonite clay and obtained CO, CO_2, and SO_2 adsorption capacity of 0.1 mmol/g, 0.44 mmol/g, and 1.02 mmol/g, respectively. Benkacem et al. [24] studied the adsorption of C_2H_2, N_2, CH_4, O_2, CO_2, and CO over halloysite, kaolinite, and montmorillonite and found that the adsorption capacities over these adsorbents were low (0.03–0.06 mmol/g). Diatomite is a siliceous sedimentary rock made from the skeletons of aquatic plants [25]. Amorphous silica is the main component of diatomite, and additionally, some metal oxides, clays, and salts are found. Diatomite shell has a high porosity thanks to the presence of a regular pattern of tiny holes. It is has been widely used as drug carriers, filter aid, and adsorbents [25–27]. Bello et al. [28] modified diatomaceous Earth with manganese oxide and found that the MnO-modified diatomite exhibited high removal efficiency of Zn, Cu, Pb, Ni, and Cd. Medjdoubi et al. [29] reported that the local diatomite treated with HCl showed a high dye adsorption capacity of 39.89 mg Janus Green B/g diatomite. Lamastra et al. [30] silanized diatomite surface with bis (triethoxysilylpropyl) disulfide, used as a highly efficient rubber reinforcement filler due to its ability to form chemical bonds with elastic molecules during vulcanization. Yuan et al. [31] reported that the surface functionalization diatomite with APTES increased Cu (II) adsorption efficiency by more than 13 times as compared to that of the original diatomite.

To the best of our knowledge, CO adsorption on diatomite has not been studied. In this paper, we report the treatment of diatomite with HCl, followed by modification with CuCl using an "atomic implantation" method. We performed CO adsorption on modified samples at different temperatures of 20°C, 30°C, and 40°C. We found that the effectiveness of Cu^+ adsorptive sites plays an important role in the CO adsorption capacity of CuCl-modified diatomite.

2. Materials and Methods

2.1. Acid Treatment of Diatomite. Raw diatomite from Lam Dong Province, Vietnam, was used in this investigation. Acid treatment was done by mixing the diatomite with HCl of 1 M concentration. The ratio of diatomite to HCl was fixed as 1 g diatomite to 20 mL of HCl solution (1 M). The mixture was then magnetically stirred at room temperature for 1 h under reflux condition. The mixture was filtered to separate diatomite from solution. Solid product was washed with distillate water until pH of 7 and then dried in an oven at 100°C for 5 h.

2.2. CuCl Modification of Diatomite. An atomic implantation method was used to modify diatomite with CuCl (denoted as CuCl/diatomite). The CuCl/diatomite materials were synthesized in a tubular reactor that has two compartments, separated by a film of quartz fibers. A certain amount of diatomite and CuCl was introduced into each compartment. After that, tubular reactor was placed in a quartz reactor and the N_2 gas stream was blown through to expel the oxygen in the reactor. The reaction system was heated to 450°C with a heating rate of 10°C/min. At this temperature, CuCl is dissociated into Cl^- and Cu^+ ions and is fed into a diatomite carrier by a stream of N_2 gas (60 mL/min) to form CuCl/diatomite material (Scheme 1). After one hour of keeping the reaction system at 450°C, the reaction system was cooled down to room temperature.

Diatomite modified with 1, 2, and 3 times CuCl was denoted as follows: 1CuCl/diatomite, 2CuCl/diatomite, and 3CuCl/diatomite.

2.3. Characterization of Diatomite and CuCl/Diatomite Samples. XRD patterns of diatomite and CuCl/diatomite were measured on D8 advance diffractometer (Bruker, Germany). The morphology of CuCl/diatomite was characterized by scanning electron microscopy (SEM, JEOL JSM 6500F) and transmission electron microscopy (JEOL JEM 1400). Transmission electron microscopy studies were performed using a JEOL JEM 1400 at 200 kV acceleration voltage. The composition of CuCl/diatomite samples was determined by energy dispersive spectroscopy (JEOL JED-2300 spectrometer). The FTIR of diatomite and CuCl/diatomite measurement was performed using a Jacos 4700 spectrometer. The Tristar-3000 adsorbent device with N_2 adsorbent was used to determine the surface area, total capillary volume, and capillary diameter of CuCl/diatomite materials. CO-TPR of CuCl/diatomite samples was performed on an AutoChem II 29020 (USA) instrument-micromeritics coupled with a thermal conductor detector (TCD). XPS analysis of CuCl/diatomite was measured using a Thermo ESCALAB spectrometer (USA) employing a monochromic Al Kα source at 1486.6 eV.

2.4. CO Adsorption Measurements. Before the adsorption measurements, the samples were degassed under vacuum at 150°C for 4 h. CO adsorption isotherms were measured at 20°C, 30°C, and 40°C using astatic volumetric apparatus (NOVE1000 e, Quantachrome Inc., Boynton Beach, FL, USA). High-purity CO (99.99%) was used for the adsorption measurements. The adsorption temperatures were controlled by a glycol water circulating bath.
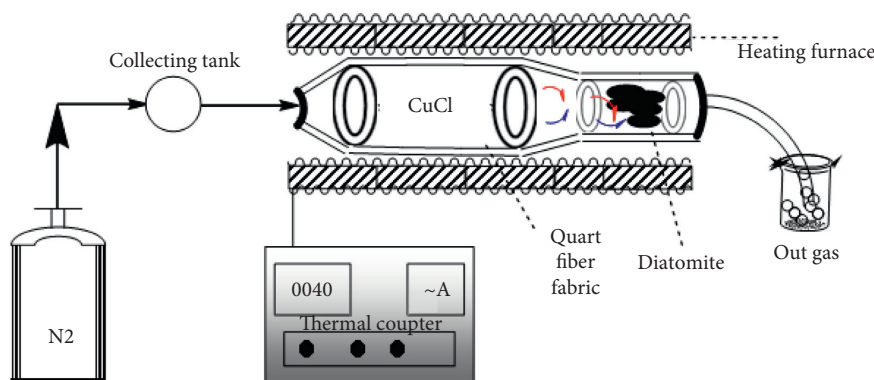
Scheme 1: Scheme of modifying CuCl/diatomite by "atomic implantation" method.

3. Results and Discussion

3.1. Structural Characterization of CuCl/Diatomite. XRD patterns of CuCl-modified diatomite samples are presented in Figure 1. In the XRD pattern of diatomite appeared the peak at 21.98°, which is characteristic for cristobalite of diatomite phase [32, 33]. In XRD patterns of CuCl-modified diatomites, the peaks at 28°, 33°, 45°, and 56° were assigned to (111), (200), (220), and (311) of CuCl phase, respectively [34]. In addition, the increase in those peak intensities with increasing the CuCl content was observed, indicating the enhancement of crystallinity.

The FTIR spectra of diatomite and CuCl-modified diatomites are presented in Figure 2. In the FTIR spectrum of diatomite appeared to the bending vibration of Si–O–Si groups at 466 cm−1, symmetric stretching vibration at 795 cm−1 of Si–O groups, and asymmetric vibration at 1091 cm−1, of Si–O groups respectively. The band at 3453 cm^{-1} is attached to the stretching vibration of Si–OH groups [35, 36]. In the FTIR spectra of CuCl-modified diatomites, the bands that are characteristic for diatomite were also observed. The additional band was observed at 669 cm^{-1}, which is attached to the stretching vibration of Si–O–Cu groups [37].

The element composition of diatomite and CuCl/diatomites determined by EDX is given in Table 1.

As seen in Table 1, with increasing the CuCl content into diatomites, O and Si content decreased from 50.48 wt% to 38.62 wt% and 36.56 wt% to 27.46 wt%, respectively, while Cl and Cu content increased from 4.74% wt to 12.3 wt% and 8.22 wt% to 21.61 wt%, respectively. This result can be explained by the fact that O and Si elements were replaced by CuCl.

EDX elemental mapping images of 2CuCl/diatomite are illustrated in Figure 3. As seen in Figure 3(c), nano Cu of 50–60 nm with uniform distribution was observed.

The SEM images of diatomite and CuCl-modified diatomites are illustrated in Figure 4.

As seen in Figure 4(a), diatomite has morphology of cylindrical in shape with a diameter of 8–12 μm and length of 5–10 μm. Diatomite is a porous material with an average pore size of 0.5 μm. The SEM image of CuCl-modified diatomites was similar to that of unmodified diatomite, and only reduction of pores was observed. In order to see better the deposition of CuCl particles on the surface and within the pore system of diatomite, we performed the analysis by using the TEM method. Figure 5 shows the TEM image of 2CuCl/diatomite. As seen in Figure 5, CuCl nanoparticles (dark color) well deposited on the surface and filled up the pores of diatomite, causing the reduction of pore size to 20–30 nm (bright color).

The N_2 adsorption-desorption isotherms of all diatomite samples exhibit a type V sorption isotherm, according to the IUPAC classification (Figure 6) [38]. The hysteresis loop observed is due to the capillary condensation of nitrogen occurred in the mesoporous channels.

Pore volume (V_{pore}), average pore diameter (D_{BJH}), and specific surface (S_{BET}) are listed in Table 2.

As observed in Table 2, surface area of CuCl-modified diatomites decreased with increasing CuCl content. This indicated the deposition of CuCl particles on adsorptive sites of diatomite, causing the decrease of N_2 adsorption capacity and consequently decreasing the surface area. Similarly, due to the deposition of CuCl particles on the pore walls of diatomite, volume pore and average pore diameter decreased with increasing the CuCl content.

CO-TPR profiles of diatomite and CuCl/diatomite samples are presented in Figure 7. In the CO-TPR profiles of CuCl-modified diatomites appeared a large peak at 438°C, which is characteristic for the reaction of Cu^+ to $Cu°$ [39, 40]. No peak at 340°C, which is typical for the reduction of Cu^{2+} to Cu^+, is noted, indicating the existence of Cu^+ ions in the CuCl-modified diatomites. Additionally, the peak intensity at 438°C increased with increasing CuCl content was observed. This proved the CO reduction of Cu^+ ions in the CuCl-modified diatomites (see Table 3). As seen in Table 3, CO reduction amount increased with increasing CuCl content (Cu^+ active sites). Thus, CO reduction amount increased from 1.42 cm^3/g to 3.78 cm^3/g with increasing Cu content from 8.22 wt% to 21.62 wt%. No CO reduction on diatomite was noted.

XPS was used to investigate the oxidation states of the copper element in the prepared 2CuCl/diatomite adsorbents. The survey XPS spectrum of 2CuCl/diatomite is presented in Figure 8. In Figure 8(a), the 2CuCl/diatomite sample showed peaks of Si 2p at 101.2 eV and 154.18 eV, O 1 s at 534.79 eV, C 1 s at 285.18 eV, Cl 2p at 198.49 eV, and
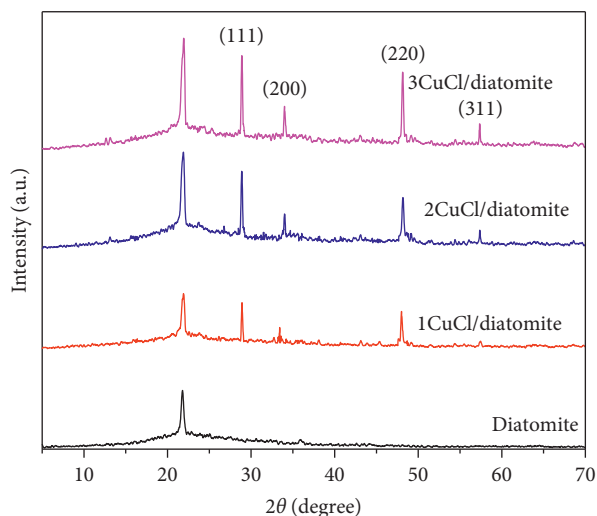
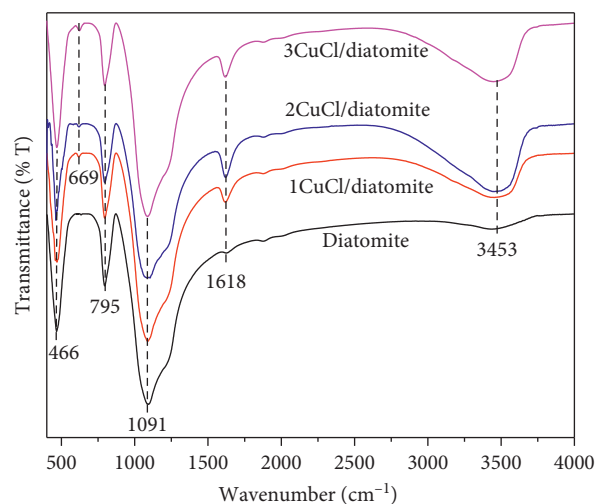Figure 1: XRD patterns of diatomite and CuCl/diatomite samples.

Figure 2: FTIR spectra of diatomite and CuCl/diatomite samples.

Table 1: Element composition (wt%) of diatomite and CuCl-modified diatomite determined by EDX.

Element	Diatomite	1CuCl/diatomite	2CuCl/diatomite	3CuCl/diatomite
O	58.18	50.48	43.09	38.62
Si	41.82	36.56	32.45	27.46
Cu	-	8.22	15.80	21.62
Cl	-	4.74	8.66	12.3
Total	100	100	100	100

Cu 2p at 936.34 eV [30, 41, 42], except for the C 1 s at 285.18 eV peak arising from adventitious hydrocarbon in the XPS instrument [42, 43]. No characteristic peak of foreign element was observed. In the Si 2p spectrum, the peak of Si 2p at 100.7 eV corresponds to Si atoms of siloxane groups, the main component of diatomite [30]. In Figure 8(c), the binding energy of O 1 s at 534.79 eV was assigned to oxygen atoms of siloxane groups (Si–O–Si) [30]. In Figure 8(d), appeared peaks at the binding energies of Cu 2p3/2 at 934.4 eV, 943.3 eV, and 963.2 eV and binding energies of Cu 2p1/2 at 953.6 eV. XPS shows that copper is presented in two oxidation states: Cu^{2+} at 962.0 eV, 956.5 eV, 943.3 eV, and 936.5 eV; characteristic peaks of Cu^{+} ions appeared at 963.8 eV, 953.3 eV, and 934.2 eV [44]. The characteristic peaks of Cu^{+} are more intense than the characteristic peaks of Cu^{2+}, and this proves the dominance of Cu^{+} content in the 2CuCl/diatomite sample.

3.2. Carbon Monoxide Adsorption on Diatomite and CuCl-Modified Diatomites.
CO adsorption isotherms of diatomite and CuCl-modified diatomite at 30°C are presented in Figure 9.
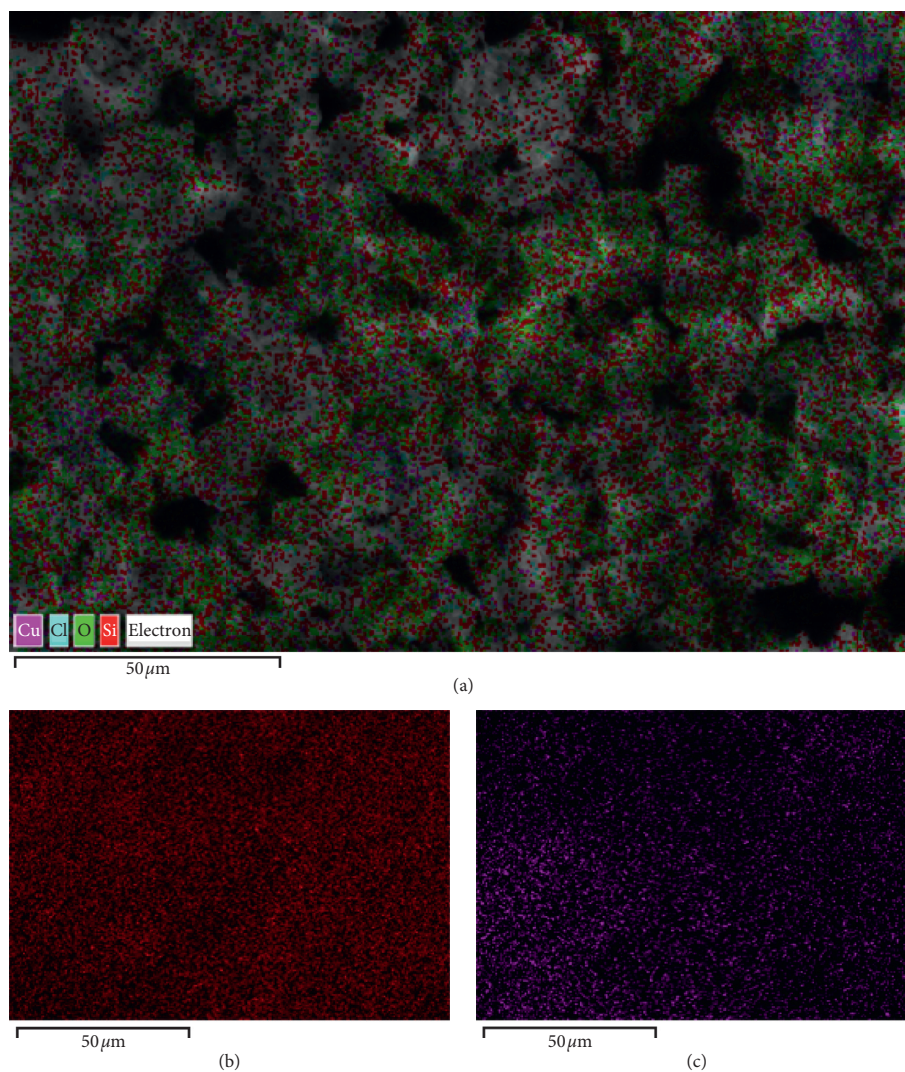
FIGURE 3: EDX elemental mapping images of 2CuCl/diatomite: (a) total elements, (b) Si element, and (c) Cu element.

As observed in Figure 9, CO adsorption capacity of CuCl/diatomites is much higher than that of unmodified diatomite. Especially, 2CuCl/diatomite showed the CO adsorption capacity of 2.96 mmol/g which was 10 times higher than that of diatomite (0.29 mmol/g). This can be attributed to the difference in the nature of CO adsorption. On the surface of diatomite, CO is physically adsorbed via van der Waals force. In contrast, CO is chemically adsorbed on CuCl-modified diatomites via the interaction between Cu^+ ions and CO to form π-complexation bonds [15]. The Cu^{2+} ions in the sample and CO are linked by the electrostatic bond and unable to form formation of the π-complexation bond [13]. The content of Cu significantly affects CO adsorption capacity. Increasing CuCl content in modified diatomites, CO adsorption capacity was from 1.7 mmol/g to 2.96 mmol/g. However, further increase of CuCl content leads to the decrease of CO adsorption capacity from 2.96 mmol/g to 2.23 mmol/g. This may be due to the agglomeration of CuCl particles which caused the low effectiveness of Cu^+ adsorptive sites and reduction of surface area [14]. Thus, effectiveness of 2CuCl/diatomite reached the

value of 1.198 CO $mmol/_{Cu\ atom}$ which was nearly twice higher than that of 3CuCl/diatomite (0.66 CO mmol/Cu atom).

Carbon monoxide adsorption isotherms of 1CuCl/diatomite, 2CuCl/diatomite, and 3CuCl/diatomite are shown in Figures 10–12. For all CuCl/modified diatomite samples (Figures 10–12), CO adsorption capacity increased with increasing the adsorption temperature from 20°C to 30°C. Further increase of adsorption temperature from 30°C to 40°C led to the decrease of the CO adsorption capacity. CO adsorption capacity on 1CuCl/diatomite at 20°C, 30°C, and 40°C was 1.55 mmol/g, 1.74 mmol/g, and 1.42 mmol/g, respectively. CO adsorption capacity on 2CuCl/diatomite at 20°C, 30°C, and 40°C was 2.63 mmol/g, 2.96 mmol/g, and 2.47 mmol/g, respectively. The above saturated CO adsorption capacity of 3CuCl/diatomite at 20°C, 30°C, and 40°C was 1.72 mmol/g, 2.23 mmol/g, and 1.59 mmol/g, respectively. Because carbon monoxide (CO) adsorption is exothermic ($\Delta H < 0$) and it is thermodynamically restricted at high temperature, one would expect that increasing adsorption temperature will lead to a decrease in the
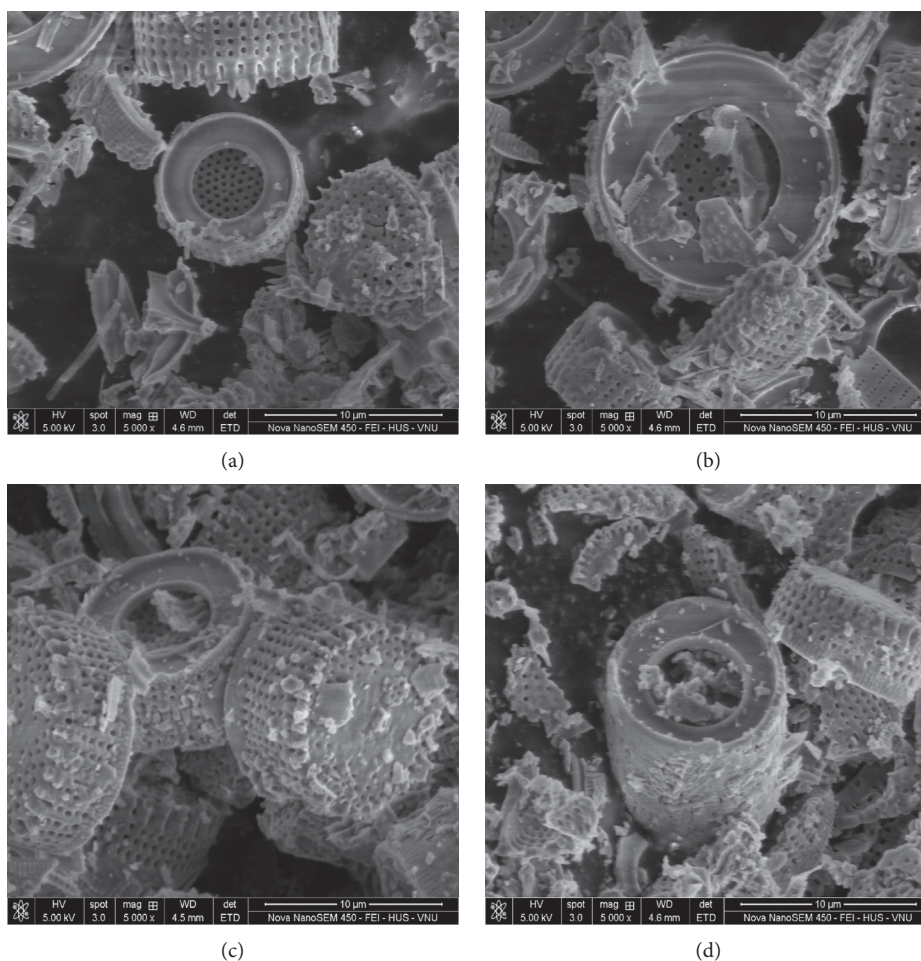
(a)

(b)

(c)

(d)

FIGURE 4: SEM images of (a) diatomite, (b) 1CuCl/diatomite, (c) 2CuCl/diatomite, and (d) 3CuCl/diatomite.
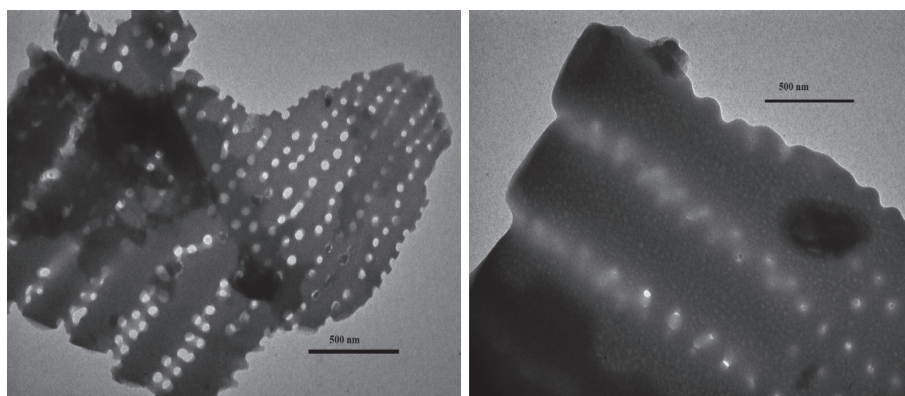

FIGURE 5: TEM image of the 2CuCl/diatomite sample.

adsorption capacity. In our case, CO adsorption behavior on Cu (I)-modified diatomites was very different. This can be rationalized as follows: when CO adsorption temperature increased from 20°C to 30°C, the diffusion to the Cu^+ adsorptive sites is promoted, resulting in the enhance of CO adsorption capacity. However, further increase of adsorption temperature leads to the decrease of carbon monoxide adsorption capacity because at high adsorption temperature

(40°C), CO desorption is favored, resulting in the decrease of carbon monoxide adsorption capacity [45].

3.3. Langmuir–Freundlich (L-F). The L-F model is applied to the adsorption isotherm of CO on CuCl/diatomite samples [46]. The L-F model can be expressed in the following representation: $q = q_m ((b.p^{(1/n)})/(1 + b.p^{(1/n)}))$ where q_m is
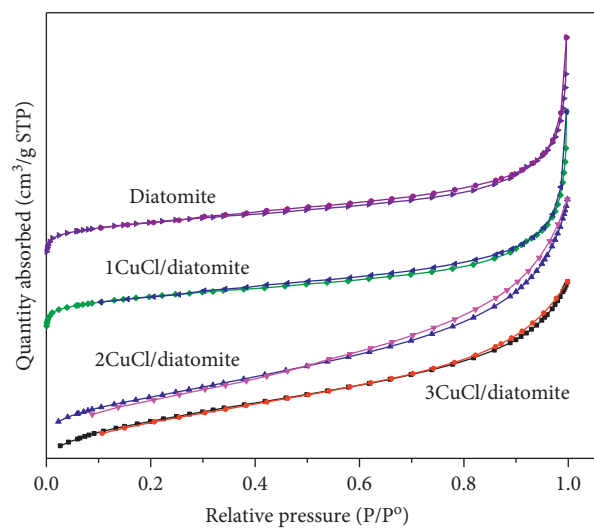
FIGURE 6: N_2 adsorption-desorption isotherms of diatomite and CuCl/diatomites.

TABLE 2: Textural properties of diatomite and CuCl-modified diatomites.

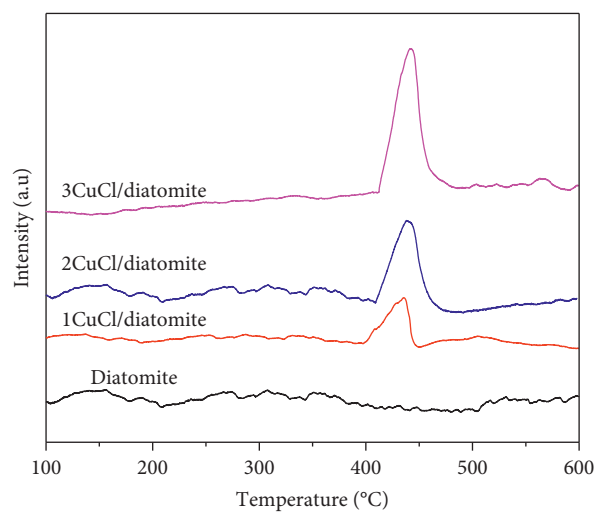| Sample	S_{BET} (m^2/g)	V Pore (cm^3/g)	D_{BJH} (nm) (average pore diameter)
Diatomite	24.34	0.117	11.7
1CuCl/diatomite	22.83	0.078	7.2
2CuCl/diatomite	18.16	0.068	6.7
3CuCl/diatomite	14.32	0.054	5.7

FIGURE 7: CO-TPR profiles of diatomite and CuCl-modified diatomites.

TABLE 3: CO reduction temperature and CO reduction amount of CuCl-modified diatomites.

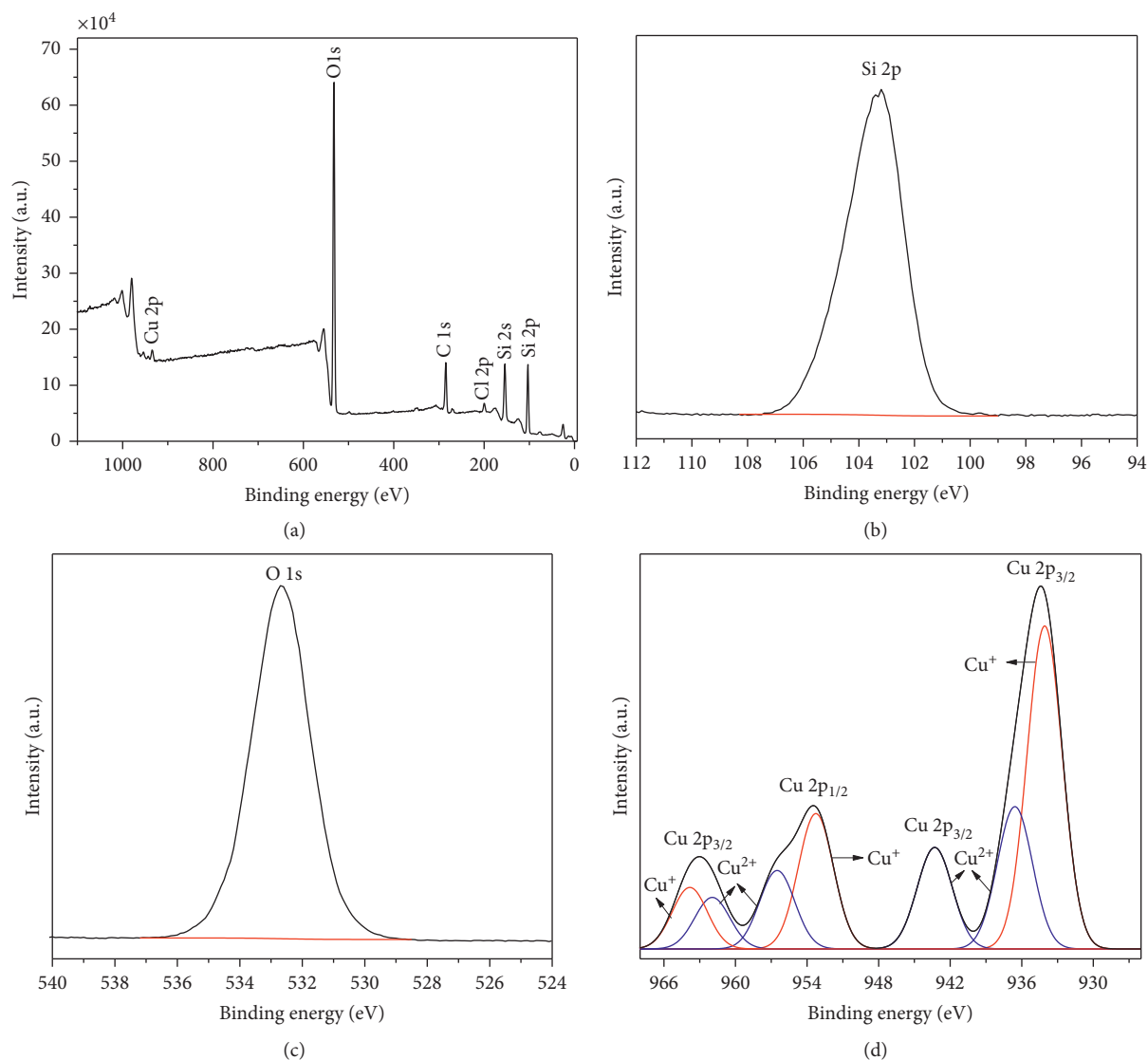| Sample	T_{max} (°C)	CO reduction amount (cm^3/g)
Diatomite	—	—
1CuCl/diatomite	438	1.42
2CuCl/diatomite	439	2.67
3CuCl/diatomite	442	3.78

FIGURE 8: XPS spectra of 2CuCl/diatomite. (a) Survey XPS spectrum of 2CuCl/diatomite, (b) XPS spectrum of Si 2p, (c) XPS spectrum of O 1 s, and (d) XPS spectrum of Cu 2p.
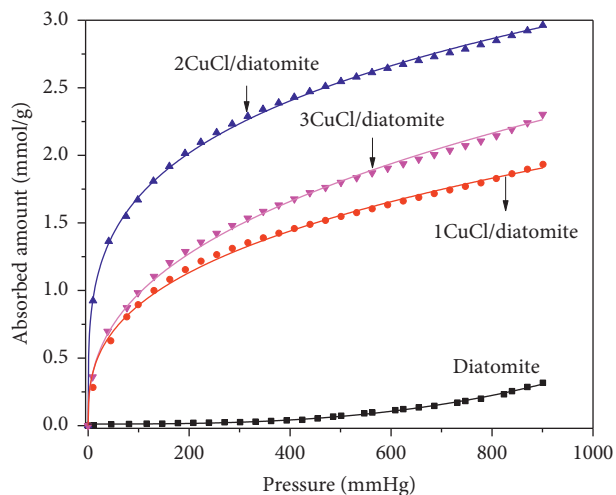

FIGURE 9: Carbon monoxide adsorption isotherms of diatomite and CuCl-modified diatomites at 30°C.
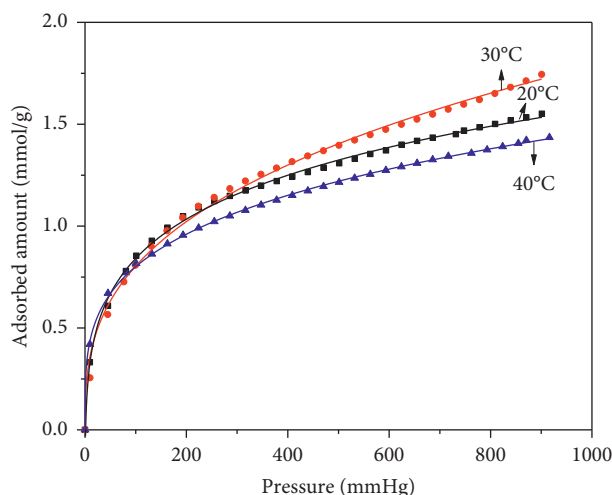
FIGURE 10: Carbon monoxide adsorption isotherms of 1CuCl/diatomite at different temperatures.
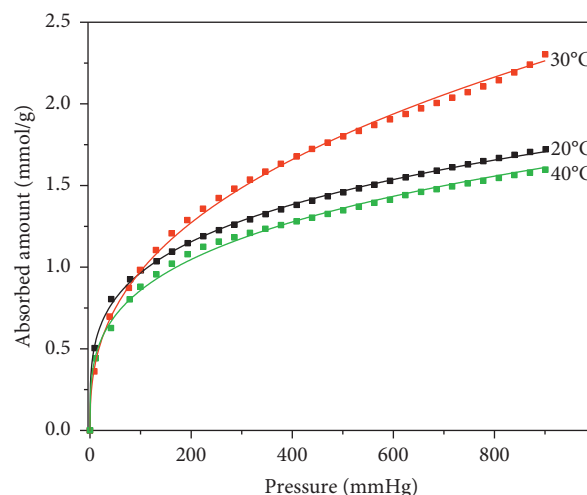

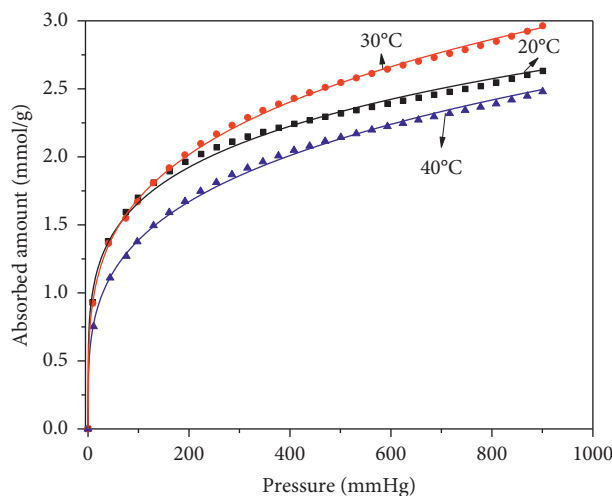FIGURE 12: Carbon monoxide adsorption isotherms of 3CuCl/diatomite at different temperatures.

FIGURE 11: Carbon monoxide adsorption isotherms of 2CuCl/diatomite at different temperatures.
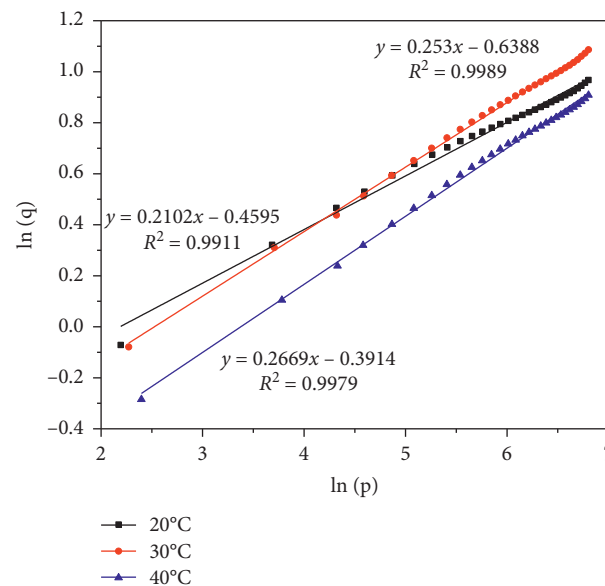
FIGURE 13: Relationship between of $\ln(q)$ and $\ln(p)$ on the 2CuCl/diatomite sample.

the saturation adsorbed amount, q is the adsorbed amount, p is the pressure, n is the corresponding deviation from the Langmuir isotherms, and b is the adsorption affinity.

Figure 13 shows the relationship between $\ln(q)$ (as a function) and $\ln(p)$ at 2CuCl/diatomite different temperatures. Langmuir–Freundlich fitting parameters of carbon monoxide isotherms on CuCl-modified diatomites are listed in Table 4.

Experimental data (Figure 13 and Table 4) show that the CO adsorption fits well with the L-F model. High R^2 values of 0.992–0.997 were obtained for all Cu (I)-modified diatomites. The highest adsorption capacity (q_m) was achieved at 30°C. Among the three samples, the 2CuCl/diatomite sample

TABLE 4: Langmuir–Freundlich fitting parameters of carbon monoxide isotherms on CuCl-modified diatomites.

Sample	Temperature (°C)	q_m (mmol/g)	b	N	R^2
	20	1.55	0.203	1.066	0.996
1CuCl/diatomite	30	1.74	0.214	1.083	0.999
	40	1.42	0.263	1.086	0.998
	20	2.63	0.206	1.011	0.995
2CuCl/diatomite	30	2.96	0.257	1.024	0.999
	40	2.48	0.260	1.046	0.998
	20	1.72	0.245	1.015	0.998
3CuCl/diatomite	30	2.23	0.235	1.021	0.998
	40	1.59	0.243	1.024	0.997

exhibited the highest carbon monoxide (CO) adsorption capacity of 2.96 mmol/g.

4. Conclusion

Modification of diatomite with CuCl was achieved by using a novel "atomic implantation" method in which CuCl was incorporated into diatomite in a vapor phase. The loading of CuCl on diatomite was varied by repeating the CuCl incorporation times.

The results are obtained from characterization using FTIR, XRD, BET, SEM-TEM, EDX, and CO-TPR. XRD revealed the presence of CuCl nanoparticles with a particle size of 50–60 nm. The CuCl particles were uniformly distributed on the surface of diatomites. CO adsorption on diatomite and CuCl-modified diatomites was evaluated. We found that modified diatomites exhibited much higher CO adsorption capacities compared to that of unmodified sample.

Among CuCl-modified diatomites, the 2CuCl/diatomite sample showed the highest carbon monoxide adsorption capacity of 2.96 mmol/g at 30°C which was 10 times higher than that of unmodified diatomite. This result can be explained on basis of the effectiveness of Cu^+ adsorption sites.

Our adsorption data showed that carbon monoxide adsorption on CuCl/diatomites fits well with the Langmuir–Freundlich model.

Data Availability

The data used to support the findings of this study are available from the corresponding author upon request.

Conflicts of Interest

The authors declare that they have no conflicts of interest.

Acknowledgments

References

[1] A. O. Goldstein, S. P. Gans, C. Ripley-Moffitt, C. Kotsen, and M. Bars, "Use of expired air carbon monoxide testing in clinical tobacco treatment settings," *Chest*, vol. 153, no. 2, pp. 554–562, 2018.

[2] M. Bergmann, M. Egert, and H. Plenio, "Malodorogenic sensing of carbon monoxide," *Chemistry—A European Journal*, vol. 23, pp. 2054–2059, 2017.

[3] E. A. Sandilands and D. N. Bateman, "Carbon monoxide," *Medicine*, vol. 44, no. 3, pp. 151-152, 2016.

[4] C. Clerbaux, P. F. Coheur, D. Hurtmans et al., "Carbon monoxide distribution from the ACE-FTS solar occultation measurements," *Geophysical Research Letters*, vol. 32, pp. 273–280, 2016.

[5] X.-F. Wu, X. Fang, L. Wu, R. Jackstell, H. Neumann, and M. Beller, "Transition-metal-catalyzed carbonylation reactions of olefins and alkynes: a personal account," *Accounts of Chemical Research*, vol. 47, no. 4, pp. 1041–1053, 2014.

[6] H. Hirai, K. Wada, and M. Komiyama, "Active Carbon-Supported copper (I) Chloride as solid adsorbent for carbon monoxide," *Bulletin of the Chemical Society of Japan*, vol. 59, no. 7, pp. 2217–2223, 1986.

[7] H. Hirai, M. Komiyama, and K. Wada, "Active carbon-supported aluminium copper chloride as water-resistant carbon monoxide adsorbent," *Chemistry Letters*, vol. 11, no. 7, pp. 1025–1028, 1982.

[8] F. Gao, Y. Wang, X. Wang, and S. Wang, "Selective CO adsorbent CuCl/AC prepared using CuCl2 as a precursor by a facile method," *RSC Advances*, vol. 6, no. 41, pp. 34439–34446, 2016.

[9] Y. Huang, "Selective adsorption of carbon monoxide and complex formation of cuprous-ammines in Cu (I) Y zeolites," *Journal of Catalysis*, vol. 30, no. 2, pp. 187–194, 1973.

[10] M.-C. Veyssiere, C. Clavaud, P. Cartraud, and A. Cointot, "Adsorption of methane +ethane and methane + carbon monoxide on molecular sieves," *Journal of the Chemical Society, Faraday Transactions 1: Physical Chemistry in Condensed Phases*, vol. 77, no. 6, pp. 1417–1424, 1981.

[11] R. Kumar, J. Mittal, N. Kushwaha, B. V. Rao, S. Pandey, and C.-P. Liu, "Room temperature carbon monoxide gas sensor using Cu doped OMS-2 nanofibers," *Sensors and Actuators B: Chemical*, vol. 266, pp. 751–760, 2018.

[12] N. Y. He, Q. H. Shi, F. Gao, Y. B. Song, Y. Yu, and H. L. Wan, "Adsorption behavior for CO on modified MCM-41 with Zn and CuCl," *Chinese Chemical Letters*, vol. 13, pp. 783–786, 2002.

[13] B. N. Manh, H. Le Giang, T. T. T. Pham et al., ""High CO performance of graphene oxide modified with CuCl by using "ion implantation" method"" *Materials Research Express*, vol. 7, 105008.

[14] C. Xue, W. Hao, W. Cheng, J. Ma, and R. Li, "CO adsorption performance of CuCl/activated carbon by simultaneous reduction-dispersion of mixed Cu (II) salts," *Materials*, vol. 12, no. 10, p. 1605, 2019.

[15] Q. Zhu, X. Wang, D. Chen et al., "Highly porous carbon xerogels doped with cuprous chloride for effective CO adsorption," *ACS Omega*, vol. 4, no. 4, pp. 6138–6143, 2019.

[16] Y. Xie, J. Zhang, J. Qiu et al., "Zeolites modified by CuCl for separating CO from gas mixtures containing CO2," *Adsorption*, vol. 3, pp. 27–32, 1996.

[17] H. Hirai, K. Wada, K. Kurima, and M. Komiyama, "Carbon monoxide adsorbent composed of copper (I) chloride and polystyrene resin having amino groups," *Bulletin of the Chemical Society of Japan*, vol. 59, no. 8, pp. 2553–2558, 1986.

[18] X. N. Pham, M. B. Nguyen, and H. V. Doan, "Direct synthesis of highly ordered Ti-containing Al-SBA-15 mesostructured catalysts from natural halloysite and its photocatalytic activity for oxidative desulfurization of dibenzothiophene," *Advanced Powder Technology*, vol. 31, no. 8, pp. 3351–3360, 2020.

[19] M. B. Nguyen and H. Giang, T. Trang et al., Novel nano-Fe2O3-Co3O4 modified dolomite and its use as highly efficient catalyst in the ozonation of ammonium solution," *Journal of Nanomaterials*, vol. 2020, Article ID 4593054, 11 pages, 2020.

[20] X. N. Pham, T. D. Pham, Ba M. Nguyen, H. T. Tran, and D. T. Pham, "Synthesis of Al-MCM-41@Ag/TiO2 nanocomposite and its photocatalytic activity for degradation of dibenzothiophene," *Journal of Chemistry*, vol. 2018, Article ID 8418605, 9 pages, 2018.

[21] X. N. Pham, D. T. Pham, Ha S. Ngo, M. B. Nguyen, and H. V. Doan, ""Characterization and application of C–TiO2 doped cellulose acetate nanocomposite film for removal of Reactive Red-195," *Chemical Engineering Communications*, vol. 1-14, 2020.

[22] J. L. Venaruzzo, C. Volzone, M. L. Rueda, and J. Ortiga, "Modified bentonitic clay minerals as adsorbents of CO, CO2 and SO2 gases," *Microporous and Mesoporous Materials*, vol. 56, no. 1, pp. 73–80, 2002.

[23] C. Volzone, J. G. Thompson, M. Alexandra, J. Ortiga, and R. Stephen, "Selective gas adsorption by amorphous clay-mineral derivatives," *Clays and Clay Minerals*, vol. 47, no. 5, pp. 647–657, 1999.

[24] T. Benkacem, B. Hamdi, A. Chamayou, H. Balard, and R. Calvet, "Physicochemical characterization of a diatomaceous upon an acid treatment: a focus on surface properties by inverse gas chromatography," *Powder Technology*, vol. 294, pp. 498–507, 2016.

[25] M. A. M. Khraisheh, M. A. Al-Ghouti, S. J. Allen, and M. N. Ahmad, "Effect of OH and silanol groups in the removal of dyes from aqueous solution using diatomite," *Water Research*, vol. 39, no. 5, pp. 922–932, 2005.

[26] R. Goren, T. Baykara, and M. Marsoglu, "Effects of purification and heat treatment on pore structure and composition of diatomite," *British Ceramic Transactions*, vol. 101, no. 4, pp. 177–180, 2002.

[27] X. Wang, S. Gao, L. Yu, and C. Miao, "Synthesis of porphyrin nanometer material by a new method," *Chemical Research in Chinese Universities*, vol. 19, pp. 854–857, 1998.

[28] O. S. Bello, K. A. Adegoke, and R. O. Oyewole, "Insights into the adsorption of heavy metals from wastewater using diatomaceous earth," *Separation Science and Technology*, vol. 49, no. 12, pp. 1787–1806, 2014.

[29] Z. Medjdoubi, M. Hachemaoui, B. Boukoussa, and R. Benhamou Hamacha, "Adsorption behavior of Janus Green B dye on Algerian diatomite," *Materials Research Express*, vol. 6, no. 8, 2019.

[30] F. R. Lamastra, S. Mori, V. Cherubini, M. Scarselli, and F. Nanni, "A new green methodology for surface modification of diatomite filler in elastomers," *Materials Chemistry and Physics*, vol. 194, pp. 253–260, 2017.

[31] Y. Peng, L. Dong, D. Y. Tan et al., "Surface silylation of mesoporous/macroporous diatomite (diatomaceous earth) and its function in Cu (II) adsorption: the effects of heating pretreatment," *Microporous and Mesoporous Materials*, vol. 170, pp. 9–19, 2013.

[32] K.-L. Lin and J.-C. Chang, *Feasibility of Recycling Waste Diatomite and Fly Ash Cosintered as Porous Ceramics*, Wiley Online Library, Hoboken, NJ, USA, 2011.

[33] M. Y. Liu, L. Zheng, G. L. Lin, L. F. Ni, and X. C. Song, "Synthesis and photocatalytic activity of BiOCl/diatomite composite photocatalysts: natural porous diatomite as photocatalyst support and dominant facets regulator," *Advanced Powder Technology*, vol. 31, no. 1, pp. 339–350, 2020.

[34] G. D. Marin, Z. Wang, G. F. Naterer, and K. Gabriel, "X-ray diffraction study of multiphase reverse reaction with molten CuCl and oxygen," *Thermochimica Acta*, vol. 524, no. 1-2, pp. 109–116, 2011.

[35] T. T. Nguyen, H. Le Giang, H. Le Chi et al., "Atomic implantation synthesis of Fe-Cu/SBA-15 nanocomposite as a heterogeneous Fenton-like catalyst for enhanced degradation of DDT," *Materials Research Express*, vol. 5, no. 11, 2018.

[36] A. Belalia, A. Zehhaf, and A. Benyoucef, "Preparation of hybrid material based of PANI with SiO2 and its adsorption of phenol from aqueous solution," *Polymer Science, Series B*, vol. 60, no. 6, pp. 816–824, 2018.

[37] G. Kour, M. Gupta, S. Paul, V. K. Rajnikant, and V. K. Gupta, "SiO2-CuCl2: an efficient and recyclable heterogeneous catalyst for one-pot synthesis of 3,4-dihydropyrimidin-2 (1H)-ones," *Journal of Molecular Catalysis A: Chemical*, vol. 392, pp. 260–269, 2014.

[38] M. D. Donohue and G. L. Aranovich, "Classification of Gibbs adsorption isotherms," *Advances in Colloid and Interface Science*, vol. 76-77, pp. 137–152, 1998.

[39] J. Wang, Z. Peng, H. Qiao et al., "Influence of aging on in situ hydrothermally synthesized Cu-SSZ-13 catalyst for NH3-SCR reaction," *RSC Advances*, vol. 4, no. 80, pp. 42403–42411, 2014.

[40] P. Da Costa, B. Modén, G. D. Meitzner, D. K. Lee, and E. Iglesia, "Spectroscopic and chemical characterization of active and inactive Cu species in NO decomposition catalysts based on Cu-ZSM5," *Physical Chemistry Chemical Physics*, vol. 4, no. 18, pp. 4590–4601, 2002.

[41] N. Yu Adonin, S. A. Prikhod'ko, A. Y. Shabalin et al., "Synthesis and structural features of nanostructured cuprous chloride with high catalytic activity," *Silicon*, vol. 7, pp. 79–87, 2015.

[42] X. N. Pham, B. M. Nguyen, H. T. Thi, and H. Van Doan, "Synthesis of Ag-AgBr/Al-MCM-41 nanocomposite and its application in photocatalytic oxidative desulfurization of dibenzothiophene," *Advanced Powder Technology*, vol. 29, no. 8, pp. 1827–1837, 2018.

[43] X. N. Pham, M. B. Nguyen, H. S. Ngo, and H. V. Doan, "Highly efficient photocatalytic oxidative desulfurization of dibenzothiophene with sunlight irradiation using green catalyst of Ag@AgBr/Al-SBA-15 derived from natural halloysite," *Journal of Industrial and Engineering Chemistry*, vol. 90, pp. 358–370, 2020.

[44] R. X. Chen, L. Zhu, J. Mao et al., "Synthesis of CuO/Co3O4 coaxial heterostructures for efficient and recycling photodegradation," *International Journal of Photoenergy*, vol. 2015, Article ID 183468, 11 pages, 2015.

[45] B. Geng, J. Cai, S. Liang, S. X. Liu, M. F. Li, and Y.-X. Chen, "Temperature effects on CO adsorption/desorption at Pt film electrodes: an electrochemical in situ infrared spectroscopic study," *Physical Chemistry Chemical Physics*, vol. 12, no. 36, pp. 10888–10895, 2010.

[46] W. Huang, X. Zhou, Q. Xia, J. Peng, H. Wang, and Z. Li, "Preparation and adsorption performance of GrO@Cu-BTC for separation of CO2/CH4," *Industrial & Engineering Chemistry Research*, vol. 53, no. 27, pp. 11176–11184, 2014.